High frequency scattering by convex curvilinear polygons

S. Langdon [⋆,*], M. Mokgolele and S. N. Chandler-Wilde [⋆]

Department of Mathematics, University of Reading, Whiteknights, PO Box 220, Berkshire RG6 6AX, UK

Abstract

We consider scattering of a time-harmonic acoustic incident plane wave by a sound soft convex curvilinear polygon with Lipschitz boundary. For standard boundary or finite element methods, with a piecewise polynomial approximation space, the number of degrees of freedom required to achieve a prescribed level of accuracy grows at least linearly with respect to the frequency of the incident wave. Here we propose a novel Galerkin boundary element method with a hybrid approximation space, consisting of the products of plane wave basis functions with piecewise polynomials supported on several overlapping meshes; a uniform mesh on illuminated sides, and graded meshes refined towards the corners of the polygon on illuminated and shadow sides. Numerical experiments suggest that the number of degrees of freedom required to achieve a prescribed level of accuracy need only grow logarithmically as the frequency of the incident wave increases.

1 Introduction

Consider the two-dimensional problem of scattering of a time-harmonic acoustic incident plane wave $u^i(\mathbf{x}) = \mathrm{e}^{\mathrm{i}k\mathbf{x}.\mathbf{d}}$ by a convex sound soft obstacle Ω, with Lipschitz boundary Γ. Here the unit vector $\mathbf{d} \in \mathbb{R}^2$ represents the direction of the incident field, and the frequency of the incident wave is proportional to the wavenumber $k > 0$. The total acoustic field u satisfies

⋆ The first and third authors gratefully acknowledge the support of Visiting Fellowships of the Isaac Newton Institute for Mathematical Sciences.

* Corresponding author.
Email addresses: s.langdon@reading.ac.uk (S. Langdon), m.mokgolele@reading.ac.uk (M. Mokgolele), s.n.chandler-wilde@reading.ac.uk (S. N. Chandler-Wilde).

$$\Delta u(\mathbf{x}) + k^2 u(\mathbf{x}) = 0, \quad \mathbf{x} \in D := \mathbb{R}^2 \backslash \bar{\Omega}, \tag{1}$$
$$u(\mathbf{x}) = 0, \quad \mathbf{x} \in \Gamma, \tag{2}$$

together with the Sommerfeld radiation condition

$$\lim_{r\to\infty} r^{1/2} \left(\frac{\partial u^s}{\partial r} - \mathrm{i}k u^s \right) = 0, \tag{3}$$

on the scattered field $u^s := u - u^i$, where $r := |\mathbf{x}|$ and the limit holds uniformly in all directions $\mathbf{x}/|\mathbf{x}|$. Existence and uniqueness of a solution $u \in C^2(D) \cap H^1_{\mathrm{loc}}(D)$ to (1)–(3) is well known - see [4, §2] for a full discussion. Using Green's theorem we have the representation [5, theorem 3.12]

$$u(\mathbf{x}) = u^i(\mathbf{x}) - \int_\Gamma \Phi(\mathbf{x}, \mathbf{y}) \frac{\partial u}{\partial \mathbf{n}}(\mathbf{y}) \, \mathrm{d}s(\mathbf{y}), \quad \mathbf{x} \in D.$$

Here $\Phi(\mathbf{x}, \mathbf{y}) := (\mathrm{i}/4) H_0^{(1)}(k|\mathbf{x} - \mathbf{y}|)$ is the fundamental solution of the two-dimensional Helmholtz equation and $\partial/\partial\mathbf{n}$ represents the derivative with respect to the unit outward normal vector $\mathbf{n}$.

Knowledge of the complementary boundary data $\partial u/\partial \mathbf{n} \in L^2(\Gamma)$ thus gives an expression for the total field at any point. Following the usual coupling procedure, we obtain the well known second kind boundary integral equation

$$(I + \mathcal{K}) \frac{\partial u}{\partial \mathbf{n}} = F, \quad \text{on } \Gamma, \tag{4}$$

where $F := 2\partial u^i/\partial \mathbf{n} + 2\mathrm{i}\eta u^i$ and, for $v \in L^2(\Gamma)$,

$$\mathcal{K} v(\mathbf{x}) := 2 \int_\Gamma \left(\frac{\partial \Phi(\mathbf{x}, \mathbf{y})}{\partial \mathbf{n}(\mathbf{x})} + \mathrm{i}\eta \Phi(\mathbf{x}, \mathbf{y}) \right) v(\mathbf{y}) \, \mathrm{d}s(\mathbf{y}).$$

Here η is a coupling parameter, with $\eta \in \mathbb{R}\backslash\{0\}$ ensuring that (4) has a unique solution [4, Theorem 2.5].

Due to the rapid oscillation of $\partial u/\partial \mathbf{n}$ when k is large, the number of degrees of freedom required to solve (4) to a prescribed level of accuracy using standard schemes, with piecewise polynomial approximation spaces, grows at least linearly with respect to the wavenumber k (see e.g. [4,9] and references therein). Much recent work has focused on reducing this cost by incorporating the high frequency asymptotics of the solution into the approximation space. In the limit as $k \to \infty$ one expects that, away from corners and shadow boundaries

(the points on the boundary where $\mathbf{n}.\mathbf{d} = 0$),

$$\frac{1}{k}\frac{\partial u}{\partial \mathbf{n}} \to \Psi := \begin{cases} \frac{2}{k}\frac{\partial u^i}{\partial \mathbf{n}} & \text{in the illuminated region, for which } \mathbf{n}.\mathbf{d} < 0, \\ 0 & \text{in the shadow region, for which } \mathbf{n}.\mathbf{d} > 0. \end{cases}$$

Thus writing

$$\frac{1}{k}\frac{\partial u}{\partial \mathbf{n}}(\mathbf{x}) = \mathrm{e}^{\mathrm{i}k\mathbf{x}.\mathbf{d}} w(\mathbf{x}), \quad \mathbf{x} \in \Gamma, \tag{5}$$

in (4) leads to a second kind boundary integral equation for a new unknown function w, which is more amenable to approximation by piecewise polynomials for large k than $\partial u/\partial \mathbf{n}$, since it approaches a constant in the illuminated and shadow regions (away from corners and shadow boundaries) as $k \to \infty$.

This approach was first attempted in [1], for problems of scattering by smooth convex obstacles, with numerical results and analysis suggesting that the number of degrees of freedom required to maintain accuracy need only grow with order $k^{1/3}$ as k increases (compared to order k for standard schemes). Combining this approach with a mesh refinement, concentrating the degrees of freedom near the shadow boundary, it appears that the order $k^{1/3}$ requirement can be removed altogether. A rigorous analysis in [6] demonstrates that increasing the number of degrees of freedom with order $k^{1/9}$ is sufficient to maintain accuracy, and numerical results in [2,6,7] (the latter with the advantage of a sparse linear system) suggest that a prescribed level of accuracy can be achieved with a number of degrees of freedom that is independent of k.

The schemes of [1,2,6,7] all assume smooth Γ and perform poorly if Γ has corners, since in this case the oscillatory behaviour of the field diffracted by the corners is not well represented by the function Ψ. The simplest obstacle with corners, a straight-sided convex polygon, is considered in [4]. Rather than using (5) in (4), one can instead rewrite the unknown function $\partial u/\partial \mathbf{n}$ as

$$\frac{1}{k}\frac{\partial u}{\partial \mathbf{n}}(\mathbf{x}(s)) = \Psi(\mathbf{x}(s)) + \mathrm{e}^{\mathrm{i}ks} v_+(s) + \mathrm{e}^{-\mathrm{i}ks} v_-(s), \quad s \in [0, L], \tag{6}$$

where $\mathbf{x}(s)$ denotes arc-length parametrisation on Γ, with L the total length of the boundary, and $v_\pm$ are to be determined. For the particular case of a straight-sided convex polygon, a consideration in [4] of a related set of half plane problems demonstrates that the functions $v_\pm$ are not oscillatory; their derivatives are highly peaked near the corners of the polygon, but rapidly decaying away from the corners. The oscillatory nature of $\partial u/\partial \mathbf{n}$ is thus represented exactly in (6) by the known leading order term Ψ and the terms $\mathrm{e}^{\pm \mathrm{i}ks}$, and to approximate $\partial u/\partial \mathbf{n}$ all that is required is to approximate the

smooth functions $v_\pm$. These functions decay sufficiently quickly that the number of degrees of freedom required to maintain the accuracy of their best L^2 approximation from a space of piecewise polynomials supported on a specific graded mesh, with a higher concentration of mesh points closer to the corners of the polygon, grows only logarithmically with respect to k as $k \to \infty$. This appears to be the best rigorous numerical analysis result to date for a problem of scattering by bounded obstacles.

In this paper, we consider the case where the scatterer has curved sides, meeting at corners. In this case, using the formulation (6) directly would not be appropriate, as the terms $v_\pm$ would still oscillate. Instead, a slightly different approach is required, combining the ideas of (5) and (6). We now write the unknown function $\partial u/\partial \mathbf{n}$ as

$$\frac{1}{k}\frac{\partial u}{\partial \mathbf{n}}(\mathbf{x}(s)) = \mathrm{e}^{\mathrm{i}k\mathbf{x}(s).\mathbf{d}} w(s) + \mathrm{e}^{\mathrm{i}ks} v_+(s) + \mathrm{e}^{-\mathrm{i}ks} v_-(s), \quad s \in [0, L], \tag{7}$$

where again $\mathbf{x}(s)$ denotes arc-length parametrisation on Γ, and now the functions w and $v_\pm$ must each be determined. Our rationale behind this representation is that the oscillatory behaviour of the "reflected field" (the scattered field in the absence of diffraction) will be well represented by $\mathrm{e}^{\mathrm{i}k\mathbf{x}(s).\mathbf{d}}$, and the oscillatory behaviour of the "diffracted field" travelling along each side of the obstacle away from the corners will be well represented by $\mathrm{e}^{\pm \mathrm{i}ks}$. We know, from results in [1,2,6,7], that in the absence of corners the representation (7) will work well, with $v_\pm = 0$ and w slowly oscillating away from shadow boundaries. Further, from results in [4] we know that if the polygon has straight sides then the representation (7) again works well, with $v_\pm$ and $w(s) = \mathrm{e}^{-\mathrm{i}k\mathbf{x}(s).\mathbf{d}}\Psi(\mathbf{x}(s))$ all non oscillatory, and $v_\pm$ highly peaked near the corners and rapidly decaying away from the corners.

In the next section we describe our Galerkin boundary element method. The approximation space we use consists of the products of plane waves $\mathrm{e}^{\mathrm{i}k\mathbf{x}(s).\mathbf{d}}$ with piecewise polynomials supported on a uniform mesh on the illuminated sides (to approximate w in (7)), together with the products of plane waves $\mathrm{e}^{\pm \mathrm{i}ks}$ with piecewise polynomials supported on graded meshes on each side of the polygon, with these meshes graded towards the corners (to approximate $v_\pm$ in (7)). In §3 we demonstrate via numerical experiments that this approach only appears to require a logarithmic increase in the number of degrees of freedom, with respect to k, in order to maintain accuracy as k increases. Finally in §4 we present some conclusions.

For simplicity we assume that $\mathbf{n}.\mathbf{d} \neq 0$, i.e. we assume that the "shadow boundary" between the illuminated and shadow sides occurs at a corner, with no grazing incidence. If this were not the case, special care would be needed in the "transition zone" around the shadow boundary $\mathbf{n}.\mathbf{d} = 0$ (see e.g. [2,6]).

2 The Galerkin boundary element method

We begin by defining some notation, as in Figure 1. We write the boundary

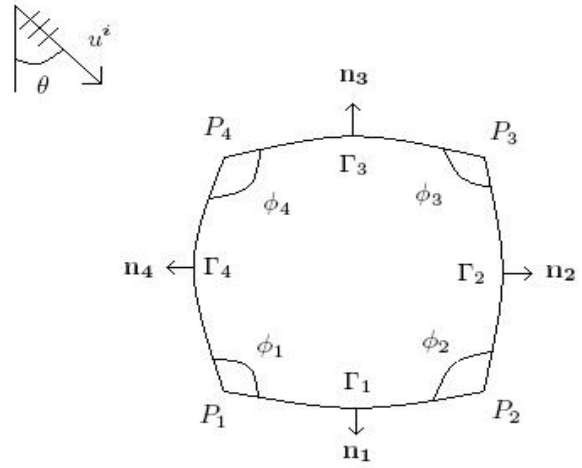

Fig. 1. Scattering by a curvilinear polygon

of the polygon as $\Gamma = \cup_{j=1}^{n}\Gamma_j$, where Γ_j, $j = 1, \ldots, n$ are the n sides of the polygon, ordered so that Γ_j, $j = 1, \ldots, n_s$, are in shadow and Γ_j, $j = n_s + 1, \ldots, n$, are illuminated, with j increasing anticlockwise as shown in Figure 1. We denote the corners of the polygon by P_j, $j = 1, \ldots, n$, and we set $P_{n+1} = P_1$, so that for $j = 1, \ldots, n$, Γ_j is the curve joining P_j with P_{j+1}. We denote the length of Γ_j by L_j, the internal angle at each vertex P_j by $\phi_j \in [0, \pi]$ (the angle between the tangents to Γ_{j-1} and Γ_j at P_j), the normal derivative to the curve Γ_j by $\mathbf{n}_j(s)$, $s \in [\tilde{L}_{j-1}, \tilde{L}_j]$, where $\tilde{L}_j := \sum_{m=1}^{j} L_m$, and the angle of the incident plane wave, as measured anticlockwise from the downward vertical, by $\theta \in [0, 2\pi)$. Writing $\mathbf{x} = (x_1, x_2)$ we then have $u^i(\mathbf{x}) = \mathrm{e}^{\mathrm{i}k(x_1 \sin\theta - x_2 \cos\theta)} = \mathrm{e}^{\mathrm{i}k\mathbf{x}.\mathbf{d}}$, where $\mathbf{d} := (\sin\theta, -\cos\theta)$.

If we denote $\boldsymbol{\gamma}_j(s)$, for $j = 1, ..., n$, as the arc-length parametrisation of the curve Γ_j, then $\mathbf{x} \in \Gamma$ can be represented by $\mathbf{x}(s) = P_j + \boldsymbol{\gamma}_j(s - \tilde{L}_{j-1})$, for $s \in [\tilde{L}_{j-1}, \tilde{L}_j]$, $j = 1, ..., n$. We rewrite (4) in arc-length parametrised form as

$$(I + K)\phi(s) = f(s), \quad s \in [0, L], \tag{8}$$

where $\phi(s) := \frac{1}{k}\frac{\partial u}{\partial \mathbf{n}}(\mathbf{x}(s))$, $L := \tilde{L}_n$, $f(s) := F(\mathbf{x}(s))$ and, for $v \in L^2[0, L]$,

$$Kv(s) := 2\int_0^L \left(\frac{\partial \Phi(\mathbf{x}(s), \mathbf{x}(t))}{\partial \mathbf{n}(\mathbf{x}(s))} + \mathrm{i}\eta\Phi(\mathbf{x}(s), \mathbf{x}(t)) \right) v(t)\, \mathrm{d}t.$$

We now define our approximation space $V_{N,\nu}$. Denoting the wavelength by

$\lambda := 2\pi/k$, we begin by defining a graded mesh on a segment $[0, A]$, for $A > \lambda$. This is the same graded mesh as that used in [4] for the case that each Γ_j is a straight line. We use a composite mesh, with a polynomial grading on $[0, \lambda]$, with the N points accumulating near the origin, and a geometric grading on $[\lambda, A]$, with the $\hat{N}_{A,\lambda,q}$ points becoming more widely spaced away from λ, as shown in figure 2. For large N, $\hat{N}_{A,\lambda,q}$ is proportional to N.

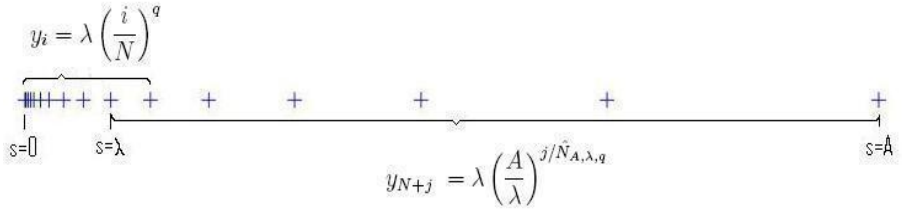

Fig. 2. Composite mesh on $[0, A]$

Definition 1 *For $A > \lambda > 0$, $q > 0$, $N = 2, 3, \ldots$, the mesh $\Lambda_{N,A,\lambda,q} := \{y_0, \ldots, y_{N+\hat{N}_{A,\lambda,q}}\}$ consists of the points*

$$y_i = \lambda \left(\frac{i}{N}\right)^q, \quad i = 0, \ldots, N,$$

together with the points

$$y_{N+j} := \lambda \left(\frac{A}{\lambda}\right)^{j/\hat{N}_{A,\lambda,q}}, \quad j = 1, \ldots, \hat{N}_{A,\lambda,q},$$

where $\hat{N}_{A,\lambda,q}$ is the smallest positive integer $\geq -\log(A/\lambda)/(q\log(1-1/N))$ (to ensure a smooth transition between the meshes, see [4]).

It follows from [4, equation (4.5)] that $\hat{N}_{A,\lambda,q} < 1 + N\log(kA/2\pi)/q$. Assuming $L_j > \lambda$, $j = 1, \ldots, n$, (if this is not the case, we use an appropriate subset of the mesh) we define $q_j := (2\nu + 3)(2\pi/\phi_j - 1)$, $j = 1, \ldots, n$, and the two meshes

$$\Gamma_j^+ := \tilde{L}_{j-1} + \Lambda_{N,L_j,\lambda,q_j}, \quad \Gamma_j^- := \tilde{L}_j - \Lambda_{N,L_j,\lambda,q_{j+1}}.$$

This choice of q_j ensures that the approximation error is evenly spread on each mesh interval, for the case of a straight sided polygon (see [4] for details). Letting $\mathrm{e}_\pm(s) := \mathrm{e}^{\pm \mathrm{i}ks}$, $s \in [0, L]$, we then define

$$V_{\Gamma_j^+,\nu} := \{\sigma \mathrm{e}_+ : \sigma \in \Pi_{\Gamma_j^+,\nu}\}, \quad V_{\Gamma_j^-,\nu} := \{\sigma \mathrm{e}_- : \sigma \in \Pi_{\Gamma_j^-,\nu}\},$$

for $j = 1, \ldots, n$, where

$$\Pi_{\Gamma_j^+,\nu} := \{\sigma \in L^2(0,L) : \sigma|_{(\tilde{L}_{j-1}+y_{m-1},\tilde{L}_{j-1}+y_m)} \text{ is a polynomial of degree } \leq \nu,$$
$$\text{for } m = 1,\ldots,N+\hat{N}_{L_j,\lambda,q_j}, \text{ and } \sigma|_{(0,\tilde{L}_{j-1})\cup(\tilde{L}_j,L)} = 0\},$$
$$\Pi_{\Gamma_j^-,\nu} := \{\sigma \in L^2(0,L) : \sigma|_{(\tilde{L}_j-\tilde{y}_m,\tilde{L}_j-\tilde{y}_{m-1})} \text{ is a polynomial of degree } \leq \nu,$$
$$\text{for } m = 1,\ldots,N+\hat{N}_{L_j,\lambda,q_{j+1}}, \text{ and } \sigma|_{(0,\tilde{L}_{j-1})\cup(\tilde{L}_j,L)} = 0\},$$

where $\{y_0,\ldots,y_{N+\hat{N}_{L_j,\lambda,q_j}}\}$ and $\{\tilde{y}_0,\ldots,\tilde{y}_{N+\hat{N}_{L_j,\lambda,q_{j+1}}}\}$ denote the points of the meshes $\Lambda_{N,L_j,\lambda,q_j}$ and $\Lambda_{N,L_j,\lambda,q_{j+1}}$ respectively.

Finally we define a uniform mesh on each illuminated side. For $j = n_s+1,\ldots,n$, the mesh $\Gamma_j^u := \{z_0,\ldots,z_{N_j^u}\}$ consists of the points

$$z_i = \tilde{L}_{j-1} + \frac{i}{N_j^u}L_j, \quad i = 0,\ldots,N_j^u.$$

Letting $\mathrm{e}_u(s) := \mathrm{e}^{\mathrm{i}k\mathbf{x}(s).\mathbf{d}}$, we then define

$$V_{\Gamma_j^u,\nu} := \{\sigma \mathrm{e}_u : \sigma \in \Pi_{\Gamma_j^u,\nu}\},$$

for $j = n_s+1,\ldots,n$, where

$$\Pi_{\Gamma_j^u,\nu} := \{\sigma \in L^2(0,L) : \sigma|_{(\tilde{L}_{j-1}+z_{m-1},\tilde{L}_{j-1}+z_m)} \text{ is a polynomial of degree } \leq \nu,$$
$$\text{for } m = 1,\ldots,N_j^u, \text{ and } \sigma|_{(0,\tilde{L}_{j-1})\cup(\tilde{L}_j,L)} = 0\}.$$

Our approximation space $V_{N,\nu}$ is then the linear span of

$$\bigcup_{\substack{j=1,\ldots,n \\ m=n_s+1,\ldots,n}} \{V_{\Gamma_j^+,\nu} \cup V_{\Gamma_j^-,\nu} \cup V_{\Gamma_m^u,\nu}\},$$

and our Galerkin method approximation $\phi_N \in V_{N,\nu}$ to the solution ϕ of (8) is defined by

$$(\phi_N,\rho) + (K\phi_N,\rho) = (f,\rho), \quad \text{for all} \quad \rho \in V_{N,\nu}, \tag{9}$$

where for $v,w \in L^2(0,L)$, $(v,w) := \int_0^L v(s)\bar{w}(s)\,\mathrm{d}s$.

For ease of exposition we consider from now on only the case $\nu = 0$. Writing ϕ_N as a linear combination of the basis functions of $V_{N,0}$, we have

$$\phi_N(s) := \sum_{j=1}^{M_N} c_j \rho_j(s), \tag{10}$$

where ρ_j is the jth basis function and M_N is the dimension of $V_{N,0}$. For $p = 1, \ldots, n$, we define $n_p^{\pm}$ to be the number of points of $\Gamma_p^{\pm}$, so $n_p^+ := N + \hat{N}_{L_p,\lambda,q_p}$, $n_p^- := N + \hat{N}_{L_p,\lambda,q_{p+1}}$, and we denote the points of $\Gamma_p^{\pm}$ by $s_{p,l}^{\pm}$, for $p = 1, \ldots, n$, $l = 1, \ldots, n_p^{\pm}$, and the points of Γ_p^u by $s_{p,l}^u$, for $p = n_s + 1, \ldots, n$, $l = 1, \ldots, N_p^u$. We denote the total number of elements supported on $\cup_{i=1}^p \Gamma_i$ by

$$M_{N,p} := \sum_{i=1}^{p} (n_i^+ + n_i^-) + \sum_{i=n_s+1}^{p} N_i^u,$$

(so that the total number of degrees of freedom is $M_N = M_{N,n}$). Then, for $p = 1, \ldots, n$, the basis functions for approximating $v_{\pm}$ in (7) are given by

$$\rho_{M_{N,p-1}+j}(s) := \frac{\mathrm{e}^{\mathrm{i}ks}}{\sqrt{s_{p,j}^+ - s_{p,j-1}^+}} \chi_{[s_{p,j-1}^+, s_{p,j}^+)}(s), \quad j = 1, \ldots, n_p^+,$$

$$\rho_{M_{N,p-1}+n_p^++j}(s) := \frac{\mathrm{e}^{-\mathrm{i}ks}}{\sqrt{s_{p,j}^- - s_{p,j-1}^-}} \chi_{[s_{p,j-1}^-, s_{p,j}^-)}(s), \quad j = 1, \ldots, n_p^-,$$

with in addition, for $p = n_s + 1, \ldots, n$, (to approximate w in (7))

$$\rho_{M_{N,p-1}+n_p^++n_p^-+j}(s) := \frac{\mathrm{e}^{\mathrm{i}k\mathbf{x}(s).\mathbf{d}}}{\sqrt{s_{p,j}^u - s_{p,j-1}^u}} \chi_{[s_{p,j-1}^u, s_{p,j}^u)}(s), \quad j = 1, \ldots, N_p^u,$$

where $\chi_{[y_1,y_2)}$ denotes the characteristic function of the interval $[y_1, y_2)$. Substituting (10) into (9) leads to a linear system of the form

$$\sum_{j=1}^{M_N} c_j \left[(\rho_j, \rho_m) + (K\rho_j, \rho_m) \right] = (f, \rho_m), \qquad \text{for } m = 1, 2, \ldots, M_N.$$

Issues regarding the efficient evaluation of the oscillatory integrals (ρ_j, ρ_m), $(K\rho_j, \rho_m)$ and (f, ρ_m) will be discussed in [8].

3 Numerical results

As a numerical example we consider scattering by a two-sided curvilinear polygon, consisting of the union of two circular segments, centred at $(\pm a, 0)$, and each of radius $r > a$, as shown in Figure 3. Specifically $\Gamma := \Gamma_1 \cup \Gamma_2$ where Γ_1 is that portion of the circle centred at $(-a, 0)$ lying to the right of the x_2-axis, and Γ_2 is that portion of the circle centred at $(a, 0)$ lying to the

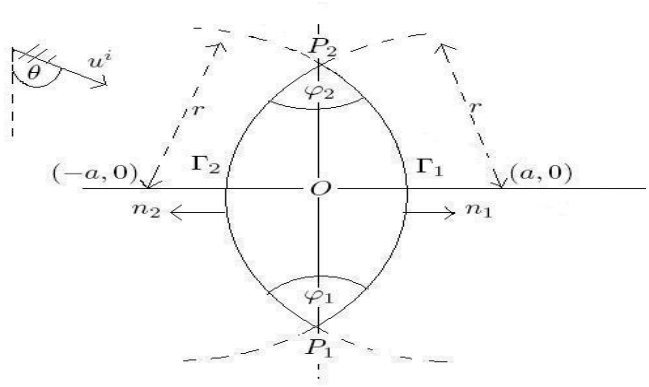

Fig. 3. Scattering by a two sided curvilinear polygon

left of the x_2-axis. The internal angles at each corner are $\varphi_i = 2\cos^{-1}(a/r)$, $i = 1, 2$, and an arc-length parametrisation of Γ is

$$\mathbf{x}(s) = \begin{cases} \left(-a + r\cos(\frac{s}{r} - \cos^{-1}\frac{a}{r}), r\sin(\frac{s}{r} - \cos^{-1}\frac{a}{r})\right), & s \in [0, 2r\cos^{-1}\frac{a}{r}), \\ \left(a + r\cos(\frac{s}{r} - 3\cos^{-1}\frac{a}{r} + \pi), r\sin(\frac{s}{r} - 3\cos^{-1}\frac{a}{r} + \pi)\right), & s \in [2r\cos^{-1}\frac{a}{r}, 4r\cos^{-1}\frac{a}{r}). \end{cases}$$

We choose $\theta = \pi/2$, $r = 3$ and $a = 1.5$, so that each side of the polygon is of length 2π and the obstacle has boundary length 4π. In our experiments we take $N_j^u = N$, $\nu = 0$, so that we are approximating by piecewise constants multiplied by plane wave basis functions on the overlapping meshes, and $\eta = -k$, this choice motivated by a desire to minimise the condition number of the resulting linear system (see [3] and the references therein for details).

In Figure 4 we plot $|\phi_N(s)|$ against $s/(2\pi)$ for $k = 10$ and for $N = 2$, 8, 32 and 128 (note the logarithmic scale for $|\phi_N(s)|$). As we expect, $|\phi_N(s)|$ is highly

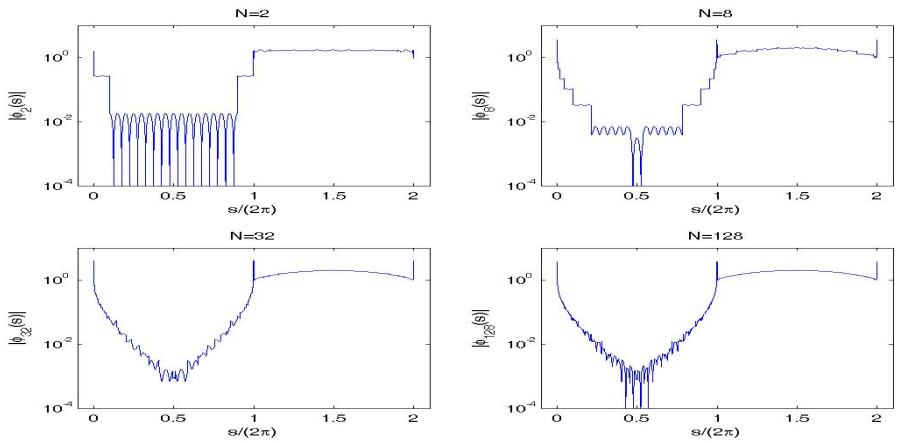

Fig. 4. Convergence for increasing N, $k = 10$

peaked at the two corners ($s = 0$ (equivalently $s = 4\pi$) and $s = 2\pi$), where ϕ is infinite. Except at these corners, $|\phi_N(s)|$ appears to be converging pointwise

as N increases. For small values of N the effect of multiplying plane wave basis functions by piecewise constants on a graded mesh can clearly be seen.

In order to test the convergence of our scheme, we take the "exact" solution to be that computed with a large number of degrees of freedom (corresponding to taking $N = 128$). For $k = 10$ and $k = 320$ the relative L^2 errors $\|\phi_{128} - \phi_N\|_2 / \|\phi_{128}\|_2$ are shown in Table 1 (all L^2 norms are computed by approximating by discrete L^2 norms, sampling at 100000 evenly spaced points on the boundary). Although no error estimate comparable with [4, Theorem 5.3] has been proved for the problem described here, we test the hypothesis that a similar estimate might hold, in which case we would expect

$$\|\phi - \phi_N\|_2 \leq CN^{-1}, \tag{11}$$

where C is a constant independent of k. The estimated order of convergence is computed as $EOC := \log_2(\|\phi - \phi_N\|_2/\|\phi - \phi_{2N}\|_2)$, and if (11) holds then we would expect to see $EOC \approx 1$. This behaviour is clearly seen in the EOC values in Table 1 for each value of k, and it is clear that $\|\phi - \phi_N\|_2$ is approximately independent of k. We also show in Table 1 the 2-norm condition

k	N	M_N	$\|\phi_{128} - \phi_N\|_2$	$\|\phi_{128} - \phi_N\|_2/\|\phi_{128}\|_2$	EOC	$\text{cond}_2 A$
10	4	28	3.6041×10^{-1}	8.4862×10^{-2}	1.0	5.89×10^{0}
	8	52	1.7839×10^{-1}	4.2005×10^{-2}	1.1	1.05×10^{1}
	16	104	8.1447×10^{-2}	1.9177×10^{-2}	0.8	7.88×10^{1}
	32	212	4.7743×10^{-2}	1.1242×10^{-2}	1.1	2.45×10^{2}
	64	420	2.2134×10^{-2}	5.2118×10^{-3}		2.49×10^{3}
320	4	36	4.0648×10^{-1}	9.6435×10^{-2}	1.0	1.66×10^{1}
	8	72	2.0592×10^{-1}	4.8853×10^{-2}	1.0	1.89×10^{1}
	16	140	1.0172×10^{-1}	2.4133×10^{-2}	1.1	2.16×10^{1}
	32	284	4.8766×10^{-2}	1.1570×10^{-2}	1.2	2.40×10^{1}
	64	568	2.1349×10^{-2}	5.0650×10^{-3}		3.32×10^{1}

Table 1
Relative errors, scattering by curvilinear polygon $k = 10$ and $k = 320$

number $\text{cond}_2 A$ of the boundary element matrix $A := [(\rho_j, \rho_m) + (K\rho_j, \rho_m)]$ for each example. Unlike methods where the approximation space is formed by multiplying standard finite element basis functions by many plane waves travelling in a large number of directions (e.g. [9]), the condition number does not grow significantly as the number of degrees of freedom increases.

In Table 2 we fix $N = 32$ and show $\|\phi_{128} - \phi_{32}\|_2$ and $\|\phi_{128} - \phi_{32}\|_2/\|\phi_{128}\|_2$ for increasing values of k. Both measures of error remain approximately constant

in magnitude as k increases, demonstrating the robustness of our scheme with respect to increasing k. Recall that keeping N fixed as k increases corresponds to keeping the number of degrees of freedom fixed for the mesh Γ_j^u, and keeping the number of degrees of freedom per wavelength fixed near each corner for the meshes $\Gamma_j^{\pm}$, whilst increasing the number of degrees of freedom away from the corners for the meshes $\Gamma_j^{\pm}$ (and hence increasing M_N) in proportion to $\log k$. Thus these results are consistent with the hypothesis that increasing M_N proportional to $\log k$ is enough to keep the error bounded. Note also that, for fixed N, $\mathrm{cond}_2 A$ does not increase as k increases. For standard schemes, the

k	M_N	$\|\phi_{128} - \phi_{32}\|_2$	$\|\phi_{128} - \phi_{32}\|_2 / \|\phi_{128}\|_2$	$\mathrm{cond}_2 A$
10	212	4.7743×10^{-2}	1.1242×10^{-2}	2.45×10^{2}
20	224	4.1460×10^{-2}	9.8064×10^{-3}	1.49×10^{2}
40	240	4.5215×10^{-2}	1.0714×10^{-2}	1.50×10^{2}
80	256	4.7159×10^{-2}	1.1183×10^{-2}	3.05×10^{1}
160	268	4.7341×10^{-2}	1.1230×10^{-2}	1.91×10^{1}
320	284	4.8766×10^{-2}	1.1570×10^{-2}	2.40×10^{1}

Table 2
Relative errors, scattering by curvilinear polygon, $N = 32$

usual requirement in the engineering literature for 10 elements per wavelength (see e.g. [9]) would lead to $20k$ degrees of freedom, i.e. 6400 degrees of freedom for the case $k = 320$ (as the obstacle has boundary length $4\pi = 2k\lambda$). By comparison, our scheme achieves approximately 1% relative error with only 284 degrees of freedom, for an obstacle with boundary of length 640 wavelengths.

Finally, in Figure 5 we plot a comparison of the solutions for $N = 128$ for $k = 5$, 10, 20 and 40. As k increases the diffracted wave is decaying faster away from the corners, i.e. the effect of the corners is becoming more localised. This behaviour mirrors closely that seen in the case of straight sided polygons [4].

4 Conclusions

We have proposed and implemented a new Galerkin boundary element method for solving problems of high frequency scattering by convex curvilinear polygons, and we have demonstrated via numerical experiments the robustness of the numerical scheme as the wavenumber increases. It appears that the number of degrees of freedom required to achieve a prescribed level of accuracy grows only logarithmically with respect to the frequency. Further details and numerical results will appear in [8].

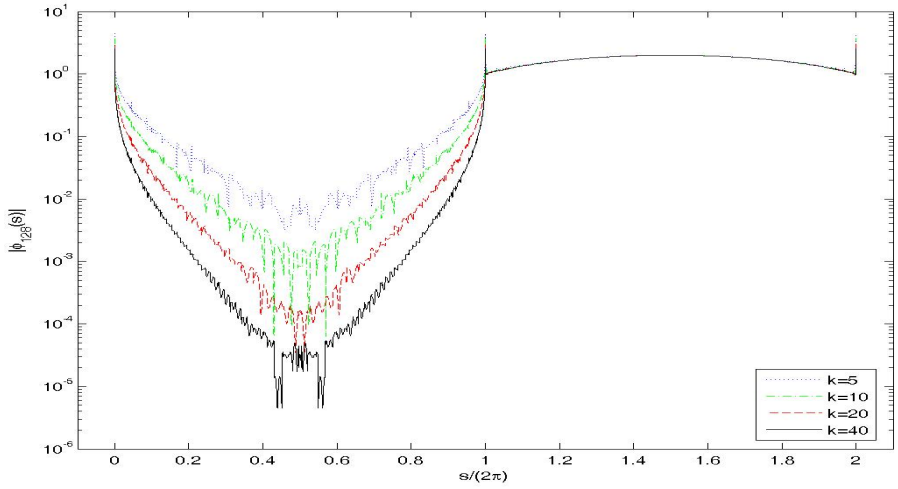

Fig. 5. Comparison of solutions for various k, each computed with $N = 128$.

References

[1] T. Abboud, J. C. Nédélec, and B. Zhou. Méthodes des équations intégrales pour les hautes fréquences. *C.R. Acad. Sci. I-Math*, 318:165–170, 1994.

[2] O. P. Bruno, C. A. Geuzaine, J. A. Monro Jr, and F. Reitich. Prescribed error tolerances within fixed computational times for scattering problems of high frequency: the convex case. *Phil. Trans. R. Soc. Lond A*, 362:629–645, 2004.

[3] S. N. Chandler-Wilde, I. G. Graham, S. Langdon and M. Lindner. Condition number estimates for combined potential boundary integral operators in acoustic scattering. Preprint NI07067, Isaac Newton Institute, October 2007.

[4] S. N. Chandler-Wilde and S. Langdon. A Galerkin boundary element method for high frequency scattering by convex polygons. *SIAM J. Numer. Anal.*, 45:610–640, 2007.

[5] D. Colton and R. Kress. *Inverse Acoustic and Electromagnetic Scattering Theory*. Springer-Verlag, 1992.

[6] V. Dominguez, I. G. Graham, and V. P. Smyshlyaev. A hybrid numerical-asymptotic boundary integral method for high-frequency acoustic scattering. *Numer. Math.* 106:471–510, 2007.

[7] D. Huybrechs and S. Vandewalle. A sparse discretisation for integral equation formulations of high frequency scattering problems. *SIAM J. Sci. Comput.*, 29:2305–2328, 2007.

[8] M. Mokgolele. *Numerical solution of high frequency scattering problems*. PhD Thesis, University of Reading (in preparation).

[9] E. Perrey-Debain, O. Lagrouche, P. Bettess, and J. Trevelyan. Plane-wave basis finite elements and boundary elements for three-dimensional wave scattering. *Phil. Trans. R. Soc. Lond. A*, 362:561–577, 2004.